



Structure and elasticity of hydrous ringwoodite: A first principle investigation

Li Li^{a,*}, John Brodholt^b, Dario Alfè^b

^a Mineral Physics Institute, Department of Geosciences, University of New York at Stony Brook, Stony Brook, NY 11790, USA

^b Department of Earth Sciences, University College London, Gower Street, London WC1E6BT, UK

ARTICLE INFO

Article history:

Received 1 March 2009

Received in revised form 16 June 2009

Accepted 7 July 2009

Keywords:

Hydrous ringwoodite

Protonation

Compressibility

First principle

ABSTRACT

First principle calculations were performed to investigate structural, IR, and elastic properties of hydrous ringwoodite and their evolution with pressure up to 36 GPa. Hydrogen defects are introduced by creating Mg- or Si-vacancies $\text{Mg}_{1.875}\text{H}_{0.25}\text{SiO}_4$, $\text{Mg}_{1.75}\text{H}_{0.5}\text{SiO}_4$ and $\text{Mg}_2\text{Si}_{0.875}\text{H}_{0.5}\text{O}_4$. Energy considerations imply that the Mg-vacancy coupled substitution will be the easiest to form, but, in the Earth, both vacancies will participate in the process. Calculated IR spectra, when compared with reported observations, suggest that both types of defects are abundant in synthetic samples. We find that $(d \ln V_S/d \ln V_P)$ for lateral variations in the H content of ringwoodite will be quite small, suggesting that this quantity will be a sensitive metric for identifying the presence of dissolved water in the transition zone.

The calculated bulk modulus decreases linearly with increasing water content with $dK/d(C_{\text{H}_2\text{O}}) = -7.1$ (GPa/wt%) at room pressure, decreasing to -6.0 (GPa/wt%) at 20 GPa. The shear modulus similarly demonstrates a decrease with increased water content given, averaged over the substitution models, by $dG/d(C_{\text{H}_2\text{O}}) = -3.0$ (GPa/wt%) at room pressure, decreasing to -1.8 (GPa/wt%) at 20 GPa. Over this pressured range, the water induce variation of $d \ln(V_S)/d \ln(V_P)$ is 0.62 at 0 GPa to 0.2 at 20 GPa.

Published by Elsevier B.V.

1. Introduction

Ringwoodite, the high-pressure polymorph of Mg_2SiO_4 , is one of the primary components of the mantle transition zone. The properties of ringwoodite directly affect our understanding of the Earth's interior between 520 and 660 km thus the whole mantle dynamics. Ringwoodite has been found to be able to host significant amounts of water up to about 2.2 wt% in the crystal structure (Bolfan-Casanova et al., 2000; Kohlstedt et al., 1996; Kudoh et al., 2000). However, the maximum amount of water ringwoodite can host is expected to be similar to that of wadsleyite (Kudoh, 2001), which can incorporate as much as 3.3 wt% water when all non-Si oxygen sites are occupied by hydroxyl (Kudoh et al., 1996; Smyth, 1994). The presence of water in ringwoodite reduces acoustic velocities (Inoue et al., 1998; Jacobsen et al., 2004; Kavner, 2003; Manghnani et al., 2005; Wang et al., 2003, 2006; Yusa et al., 2000) and thus may have large impact on the seismic velocities in the mantle transition zone. Water in ringwoodite also affects other properties such as viscosity (Chen et al., 1998) and electric conductivity (Huang et al., 2005). Bercovici and Karato (2003) hypothesize that the transition zone is highly enriched in water owing to the capacity of wadsleyite and ringwoodite to store water in their crystal structures. Such a structure in the distribution of water in the

Earth has many consequences. It becomes important to define a seismic metric that is sensitive to the water content in order to define the areas of high concentration and those of low concentrations. Though the models generated here, we propose that the seismic parameter, $(d \ln V_S/d \ln V_P)$, is such a parameter.

The incorporation of hydrogen into nominally anhydrous minerals is generally accepted as being via the creation of hydroxyl, OH^- , groups in conjunction with a cation vacancy (Ross et al., 2003). In the case of ringwoodite, this spinel-structured mineral (shown in Fig. 1) consists of interleaved octahedral and mixed octahedral-tetrahedral layers. The possible protonation sites in Mg-ringwoodite (2 wt% H_2O) can lie close to the O–O octahedral edges with the OH vector subparallel to the Mg–O (at an angle of 27.0°) with Mg–H and Si–H distances of 1.29 and 2.06 Å (Ross et al., 2003). This is similar to the view that the possible sites are between the O–O pairs around vacant octahedral 16c sites (mixed octahedral-tetrahedral layer) and 16d sites (octahedral layer) (Kudoh et al., 2000). An alternative view is that the Si–O–Si bonds and non-silicate oxygens act as the protonation sites (Chamorro Pérez et al., 2006; Kleppe et al., 2002a,b) and that the most probable site for protonation is the tetrahedral edge.

Pressure may have an effect on the proton sites in ringwoodite. A pressure-induced second-order displacive phase transitions was suggested as a merging of silicate-stretching mode (736 and 835 cm^{-1}) with pressure in hydrous ringwoodite (Kleppe et al., 2002a). This second-order phase transitions were further observed in a synchrotron IR study (Chamorro Pérez et al., 2006).

* Corresponding author. Tel.: +1 631 632 8220; fax: +1 631 632 8140.
E-mail address: lilli@ic.sunysb.edu (L. Li).

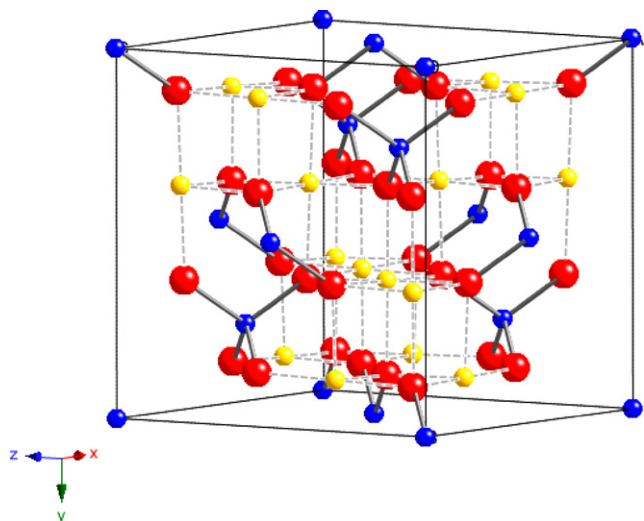


Fig. 1. Unit cell structure for Mg_2SiO_4 ringwoodite. Yellow represent Mg atoms; blue represent Si atoms; red represent O atoms. (For interpretation of the references to color in this figure legend, the reader is referred to the web version of the article.)

In addition to the experimental studies, first principle approaches have also been used to investigate the elastic and vibrational properties of water-free ringwoodite (Kiefer et al., 1997; Li et al., 2006, 2007; Yu and Wentzcovitch, 2006), plastic properties (Carrez et al., 2006) and the structure and dynamics of hydrous

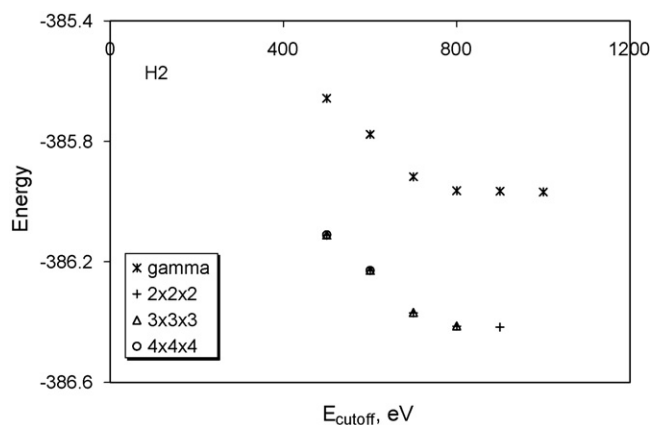


Fig. 2. Energy cutoff test for hydrous ringwoodite with 1.65 wt% H_2O . Test volume at 541.63 \AA^3 . Cut-off energy 800 eV and $2 \times 2 \times 2$ K-point are considered the converged condition. Higher cutoff energy and K-point sampling change minimum energy less than 5×10^{-5} eV/atom. Test on H4 and SiH model (3.3 wt% H_2O) lead to the same cutoff energy and K-point sampling.

ringwoodite (Haiber et al., 1997). The first principle method can be useful in investigating hydrous ringwoodite since the energetics can be calculated for a given hydrous structure and used to discriminate between different protonation sites. The current study investigates the structural and elastic properties of hydrous ringwoodite. We focus on two water contents (1.65 and 3.3 wt% H_2O). Partial disorder has been reported in hydrous ringwoodite (Kudoh et al., 2000)

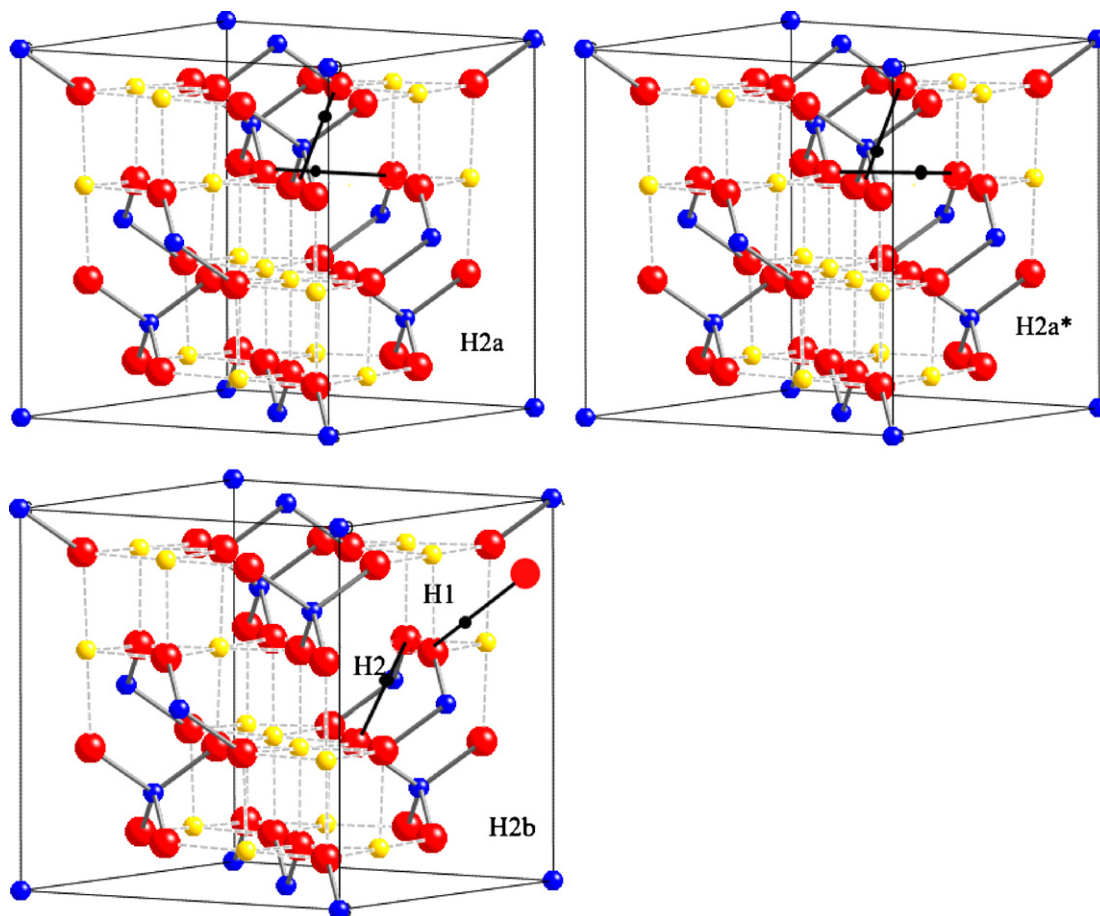


Fig. 3. Proton positions in H2 models. The black solid circles represent protons. The V_{Mg} is at $(5/8, 3/8, 3/8)$. Protons of model H2a and H2a* still attached to the same oxygen pairs but shift to a different position. One proton (H1) in model H2c is outside of the Mg-vacant octahedron. This proton (H1 in model H2c) is attached to an oxygen shown outside the unit cell box in the periodic position of another oxygen inside the box.

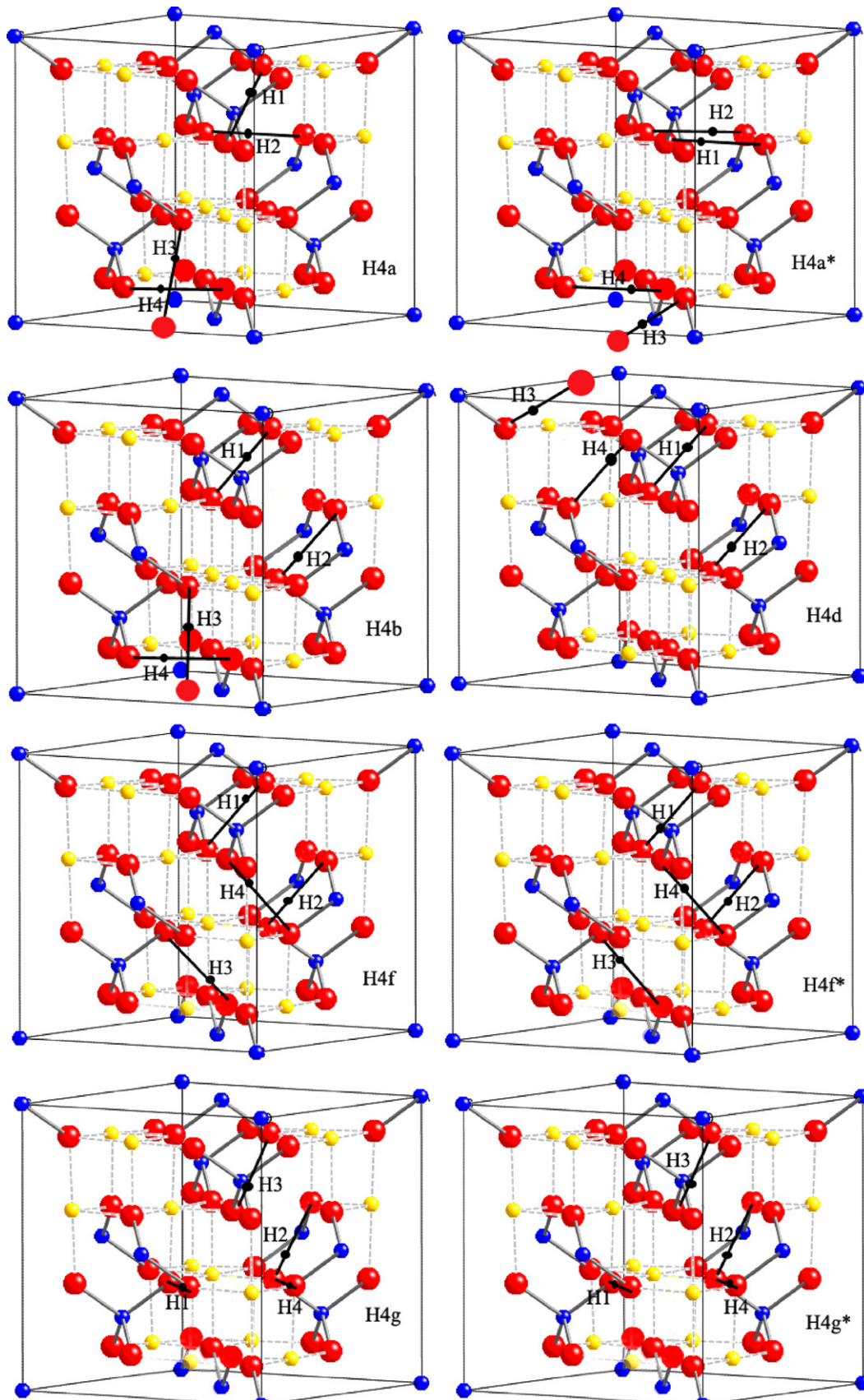


Fig. 4. Proton sites for H4 models. In model H4a and H4a*, the third proton (H3) is attached to an oxygen outside the unit cell box. This oxygen atom is in the periodic position of an oxygen atom inside the box, likewise in model H4b. The protons in model H4f and H4f* attach to the same O–O pairs but have different positions, likewise for model H4g and H4g*. Only in model H4g and H4g*, two protons (H2 and H4) are attached to the same O atom. This oxygen atom (0.6316, 0.6316, 0.3684) is shared by the two Mg-vacant octahedrons.

and can be simulated using first principle approach (Kiefer et al., 1997; Li et al., 2007). Due to the complexity, we have only reported here the hydrous spinel with ordered Mg–Si (Mg in 16d and Si in the 8a site). We aim to constrain the location of protons in ringwoodite and their evolution and effect on elasticity at pressures up to 40 GPa.

2. Methods

The calculations on hydrous Mg_2SiO_4 ringwoodite were done using *ab initio* molecular dynamics (AIMD) simulations with the VASP code (Kresse and Joubert, 1999). We used the projector-augmented-wave (PAW) (Blöchl, 1994; Kresse and Joubert, 1999) implementation of density functional theory (DFT) and the implementation of an efficient extrapolation for the charge density (Alfè, 1999) using the generalized gradient approximation, GGA. All calculations were performed using a 56-atom unit-cell. We tested the $T=0\text{K}$ equation of state for the two compositions using 800 eV and $2 \times 2 \times 2$ K-points sampling the Brillouin zone. The convergence of the energy is less than $5e-4\text{eV/atom}$ (shown in Fig. 2). A plane-wave cut-off energy 800 eV was used for high temperature simulation. The Γ point was used for sampling the Brillouin zone. The effect of larger energy cut-offs and K-point sampling on the calculated properties are found to be insignificant. The time step used in the dynamical simulation was 1 fs. The core radii are 2.0 a.u. for Mg (core configuration $1s^22s^2$), 1.9 a.u. for Si ($1s^22s^22p^6$), 1.52 a.u. for O ($1s^2$), and 1.1 a.u. for H ($1s^1$). It took at least 2 ps calculation to reach the equilibrium. Tests show that the effect of longer simulation on the calculated results is small.

Calculations on the vibrational properties are performed using a cell based on 56 atoms for Mg_2SiO_4 ringwoodite. Then Mg or Si atoms are substituted by hydrogen atoms. The computations use the local density approximation (LDA) (Ceperley and Alder, 1990; Perdew and Zunger, 1981). The equilibrated structure of hydrous ringwoodite was calculated using the first-principles implementation of a variable cell-shape damped molecular dynamics (VCSMD) (Wentzcovitch and Price, 1996; Wentzcovitch et al., 1995). Pseudopotentials of Mg and H were generated by the method of von Barth and Car (Karki et al., 2000; Tsuchiya et al., 2005), while those of O and Si are by the method of Troullier and Martins (1991). The plane-wave energy cut-off used is 70 Ry and the K-point sampling of the charge density was performed on a $2 \times 2 \times 2$ grid in Brillouin Zone shifted by $(1/2, 1/2, 1/2)$. The calculations with $2 \times 2 \times 2$ and $3 \times 3 \times 3$ grid of K-points give a difference in energy by 10^{-4} Ry/atom. The dynamical matrix was obtained using density functional perturbation theory (DFPT) (Baroni et al., 2001) only at gamma point. Phonon frequencies were obtained by diagonalizing the dynamical matrix.

3. Results and discussion

We investigated four different incorporation mechanisms, three involving the introduction of hydrogen via Mg- or Si-vacancies (Kudoh, 2001; Kudoh et al., 2000; Ross et al., 2003), and one is an interstitial mechanism (Haiber et al., 1997). The first, H2, considers the replacement of one Mg^{2+} ion by two protons. For the single 56-atom unit cell, this produces a concentration of 1.65 wt% water. The second, H4, considers the substitution of two Mg^{2+} ions by four protons in one unit cell. This allows us to evaluate the effect of proton clustering. The third, SiH, is the hydrogarnet substitution of four protons for an Si^{4+} ion. SiH and H4 both produce a water concentration of 3.3 wt%. There is only one unique Mg site (0.625, 0.625, 0.625), one Si site (0, 0, 0) and one O site (0.3684, 0.3684, 0.3684) to consider in dry ringwoodite. We use a unit cell in our simulation (56 atoms). The tested H2, H4 and SiH models are shown in Figs. 3–5.

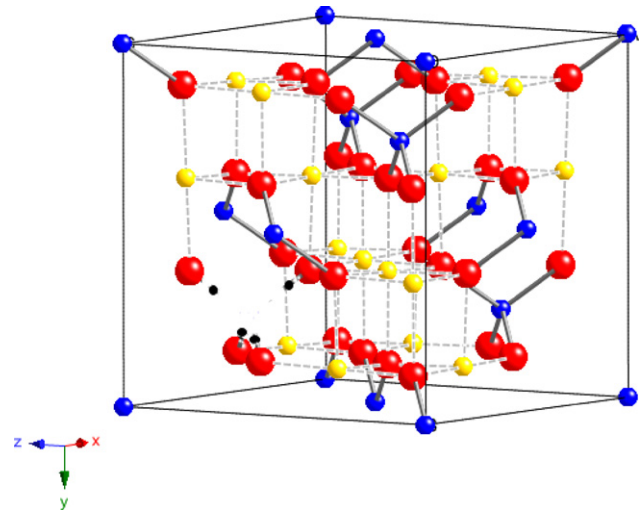


Fig. 5. Proton sites for SiH models. In this model, Si-vacancy is at (0, 0, 0). The four protons are attached to the four oxygen atoms and point to the center of the tetrahedral.

Firstly we consider a 56-atom ringwoodite cell with one interstitial proton, as was done in another study (Haiber et al., 1997). In our study, the interstitial proton relaxed to a position along the O–O edge of a Mg-octahedron. The distances of the proton from two neighboring Mg atoms are 2.05 and 2.46 Å. The H–O distance is 1.03 Å (vs. 1.07 in Haiber et al., 1997) and 1.60 Å. The distances from the proton to the close Si atoms are 2.13 and 2.35 Å. This finding is in contrast to previous reported model (Ross et al., 2003) in which the O–H bond is sub-parallel to the Mg–O bond yielding an Mg–H distance of 1.29 Å. Haiber et al. (1997) argued that at high temperature, the Mg^{2+} -vacancies and H^+ impurities will not bound to each other and, therefore, only considered the interstitial H^+ . However, we find that protons are strongly captured by the Mg-vacancy. This finding is supported by our MD calculation at high temperature (see later text). Therefore, our calculations are done using models with Mg- or Si-vacancies charged balanced by protons.

3.1. H2 model (hydrous ringwoodite with 1.65 wt% H_2O)

In this configuration, one Mg is replaced by two H atoms. We have tested 10 distinct arrangements of placing the two hydrogen atoms in the structure. On relaxation, three stable structures (model H2a, H2a* and H2b) were found (Fig. 3, Table 1). Models H2a and H2a* are similar and have both protons inside the Mg-vacant octahedron, lying close to the O...O edges of the octahedron. In contrast, the H2b model has only one proton inside the Mg-vacant octahedron; the other proton resides outside this Mg-vacant octahedron. At 0 GPa, H2b model has a higher energy ($\sim 0.6\text{eV}$) than the other

Table 1

Calculated total energy, volume and cell parameters of dry and hydrous ringwoodite at 0 GPa (1.65 wt% H_2O). The ideal Mg vacant site is (5/8, 3/8, 3/8).

	Dry	H2a	H2b
A (Å)	8.142	8.154	8.151
E (eV)	−383.3369	−386.5173	544.6300
V (Å ³)	539.77	542.22	541.60
H1– V_{Mg} (Å)	–	1.486	1.435
H2– V_{Mg} (Å)	–	1.463	5.080
O–H1 (Å)	–	1.020	1.024
O...H1 (Å)	–	1.706	1.676
O–H2 (Å)	–	1.020	1.104
O...H2 (Å)	–	1.707	1.486
H1–H2 (Å)	–	2.736	5.259

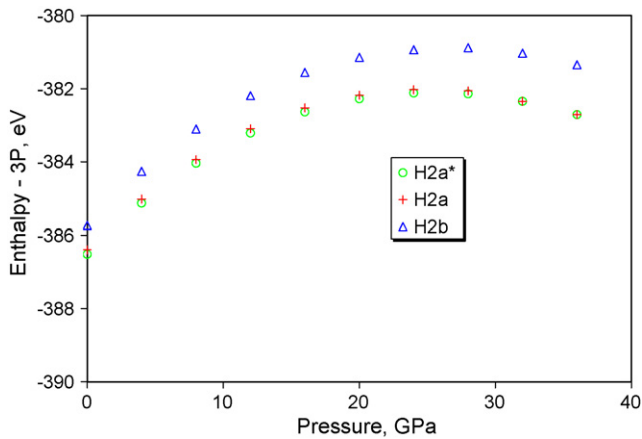


Fig. 6. Enthalpy vs. pressure for H2 models (H2a, H2a*, H2b). The enthalpy axis is represented by $H-3P$ in order to allow an expanded scale to visualize the differences between models. Model H2a represents a configuration relaxed at 0 GPa. Model H2a* represent a configuration relaxed at 36 GPa. With increasing pressure, relaxed H2a model spontaneously switches to H2a* at 24 GPa meaning a change of proton sites.

two models, suggesting that protons are prone to stay inside the Mg-vacant octahedral.

3.2. Effect of pressure on H2 models

The stable structures of model H2a and H2b were calculated up to 36 GPa. For model H2a, the calculation started with a configuration relaxed at 0 GPa. Then the same configuration H2a was used for higher pressure relaxation calculation. With increasing pressure, the H2a model spontaneously switched to model H2a* at pressure 32 GPa indicating a change of proton sites. The proton sites for model H2b remain unchanged between 0 and 36 GPa. Fig. 6 shows the enthalpy ($H-3P$ is plotted for scale convenience) versus pressure for these three models. Model H2a has a slightly higher enthalpy than model H2a* up to 36 GPa. However, the energy dif-

ferences are small (0.09–0.12 eV equivalents to a thermal energy of about 100 K) suggesting that protons can easily migrate inside the Mg-vacant octahedral in the ringwoodite structure at high temperature; this is also supported by the AIMD simulation described later.

Fig. 7 shows the H–O and Si–O atom distances for the three models. The H–O and H...O distances in models H2a and H2a* are very similar. The distances from the two protons to the nearby O atoms in model H2b are different throughout the pressure range studied. These findings suggest that pairs of protons tend to reside in locations on opposite sides of the octahedron at 0 K.

3.3. H4 model (hydrous ringwoodite with 3.3 wt% H₂O)

In a dry ringwoodite unit cell, Mg–Mg pairs have three unique distances (5.70, 4.94 and 2.85 Å). We tested various models (H4a–H4g) with pairs of protons replacing two different Mg-vacancies. A few models stabilized (model H4a–H4g, shown in Table 2). Even though the starting sites are different, model H4c finds the same oxygen hosts for the four protons as model H4b; relaxed model H4e is the same as relaxed model H4f. The four protons are found to reside in two separate Mg-vacant octahedrons in all models. H4a and H4b have an Mg–Mg-vacancy distance of 5.70 Å; H4c has an Mg–Mg-vacancy distance of 4.94 Å; H4d and H4e have an Mg–Mg-vacancy distance of 2.85 Å. The four protons lie close to the O...O edges of the Mg-vacant octahedrons in all models. The protons in model H4f and H4f* attach to the same O–O pairs but have different positions, likewise for model H4g and H4g*. Only in model H4g and H4g* are two protons (H2 and H4) attached to the same O atom. This is located at (0.6316, 0.6316, 0.3684) and is shared by the two Mg-vacant octahedrons.

3.4. Effect of pressure on H4 models

The stable structures of model H4a–H4g (shown in Fig. 4) were calculated up to 36 GPa. Fig. 8 shows the relationship between the

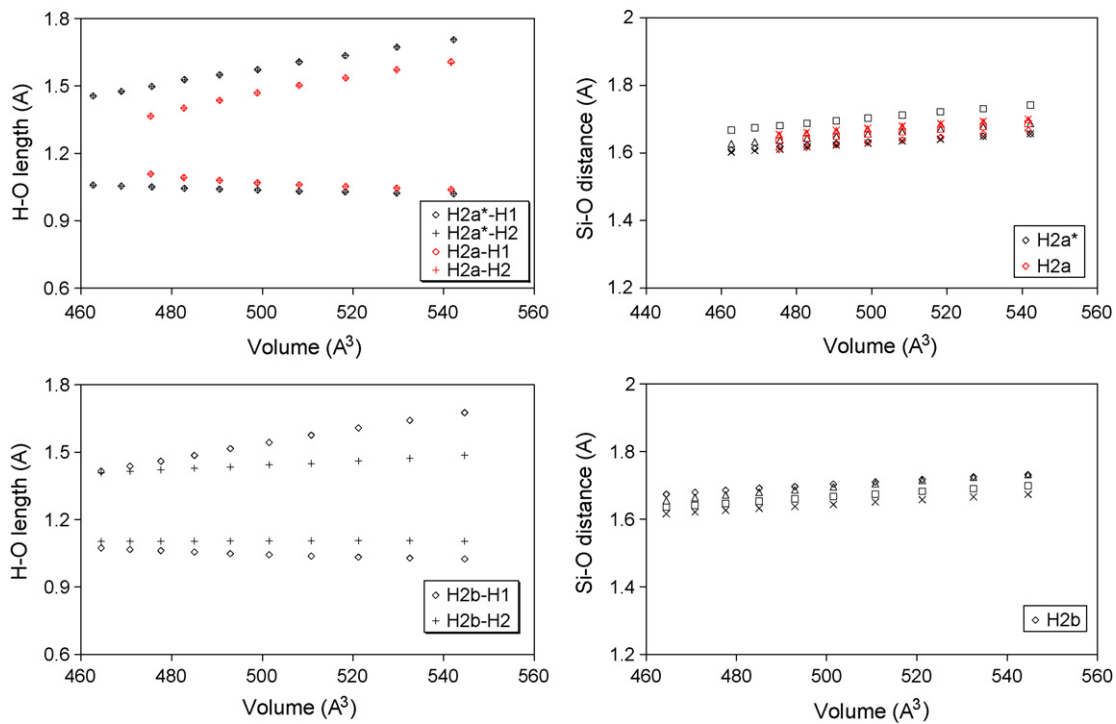


Fig. 7. Atom distances for model H2a, H2a* and H2b. A change of proton sites can be seen from the H–O and Si–O distances at volume of 468.91 Å³. H2a* has the lowest energy among the three models.

Table 2
Calculated total energy, volume and cell parameters of hydrous ringwoodite at 0 GPa (3.3 wt% H₂O). One ideal Mg1-vacancy is at (5/8, 3/8, 3/8); the other Mg2-vacancy site is listed in the table.

	H4a	H4b	H4d	H4f	H4g	SiH
A (Å)	8.165	8.169	8.165	8.162	8.166	8.166
V (Å ³)	544.43	545.06	544.25	543.80	544.61	559.80
E	-389.5741	-388.9760	-389.2831	-389.3096	-389.1934	-389.160791
V _{Mg2} site	(1/8, 7/8, 3/8)	(1/8, 7/8, 3/8)	(1/8, 1/8, 5/8)	(3/8, 5/8, 3/8)	(3/8, 5/8, 3/8)	Si(0,0,0)
V _{Mg1} - V _{Mg2} (Å)	5.70	5.70	4.94	2.85	2.85	-
H1-O (Å)	1.039	1.033	1.032	1.025	1.029	0.9570
H1···O (Å)	1.558	1.622	1.629	1.677	1.645	1.1674 (V _{Si-H})
H2-O (Å)	1.039	1.040	1.035	1.004	1.018	0.9566
H2···O (Å)	1.556	1.577	1.611	1.809	1.679	1.1632 (V _{Si-H})
H3-O (Å)	1.039	1.016	1.035	1.025	1.654	0.9566
H3···O (Å)	1.712	1.764	1.746	1.677	1.020	1.1632 (V _{Si-H})
H4-O (Å)	1.039	1.016	1.033	1.004	0.994	0.9566
H4···O (Å)	1.556	1.702	1.627	1.808	1.962	1.1632 (V _{Si-H})

enthalpy (plotted as H-3P for convenience) and pressure for these five models. The protons switch sites at elevated pressures for some models (H4a, H4f and H4g); the new sites are labeled as model H4a*, H4f* and H4g*, while the proton sites for model H4b and H4d remain unchanged between 0 and 36 GPa as shown in Fig. 8a–d. There is no apparent trend between the enthalpy and the V_{Mg} - V_{Mg} distance since H4a and H4a* are the highest and lowest enthalpy models while the other four models have intermediate enthalpy at all pressures but still H4a seems to be the lowest enthalpy. The total enthalpy difference among the five models decreases with pressure but is resolvable at 36 GPa.

The energy difference between H4a and H4a* ranges from 0.88 to 1.00 eV up to 36 GPa, which correspond to a thermal energy of 200 K. The protons switch to a different oxygen host in model H4a to form model H4a*; but it is less likely for model H4a* to switch back due to large different total energy. The energy differences between

H4f and H4f* is ~0.2–5 eV. The energy differences between H4g and H4g* range from 0.06 to 0.12 eV. These results indicate that it requires the least amount energy to disorder protons between the two sites along the O–O edge, which is most likely to occur at the Earth conditions.

Fig. 9 shows the H–O and Si–O atom distances for the five models. It can be clearly seen that the proton sites transition results in the H–O and Si–O distances change in model H4a, H4f and H4g. The four protons tend to have similar H–O distances but different H···O distances. The effect of pressure on the H–O and Si–O distance is small compared with the H···O distance.

3.5. SiH model (hydrous ringwoodite with 3.3 wt% H₂O)

We tested SiH models with four protons replacing one Si atom and being attached to different oxygen atoms. The stable structures

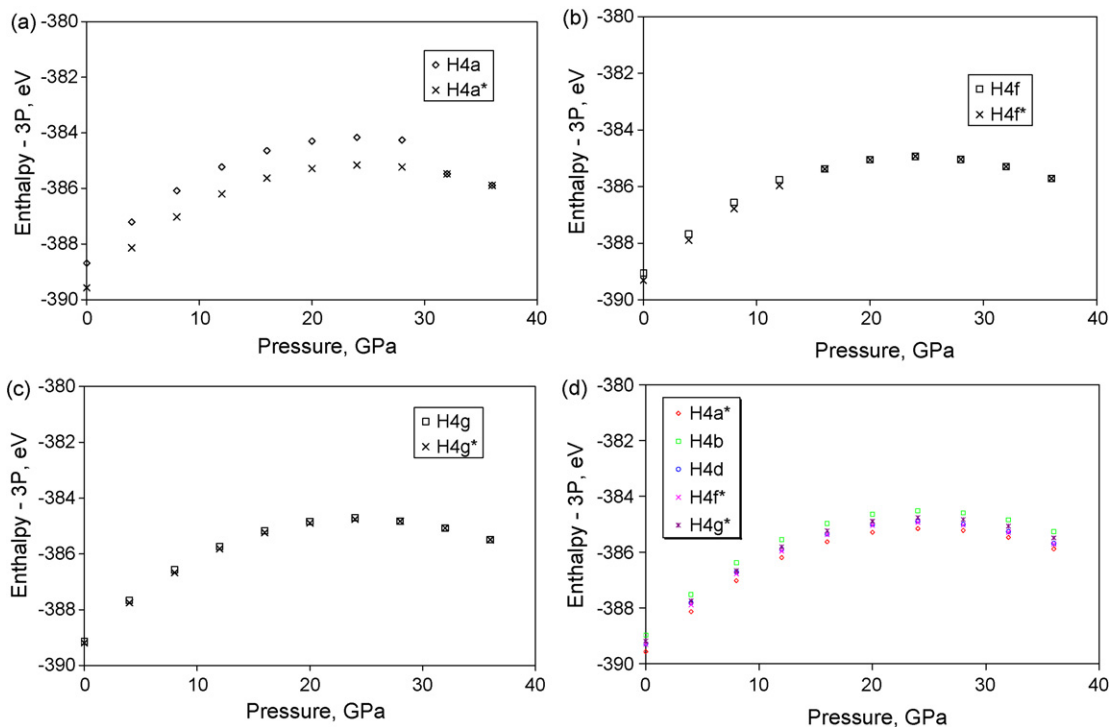


Fig. 8. (a–d) Enthalpy vs. pressure for H4 models (H4a, H4b, H4d, H4f, and H4g). The enthalpy axis is represented by H-3P in order to allow an expanded scale to visualize the differences between models. Model H4a represents a configuration relaxed at 0 GPa. Model H4a* represent a configuration relaxed at 36 GPa. With increasing pressure, relaxed H4a model spontaneously switches to H4a* at 32 GPa meaning a change of proton sites. Similar situations are for H4f and H4g. The proton sites of Model H4b and H4d remain unchanged between 0 and 36 GPa. (d) Shows the fitted enthalpy–pressure curves for models H4a*, H4b, H4d, H4f* and H4g*.

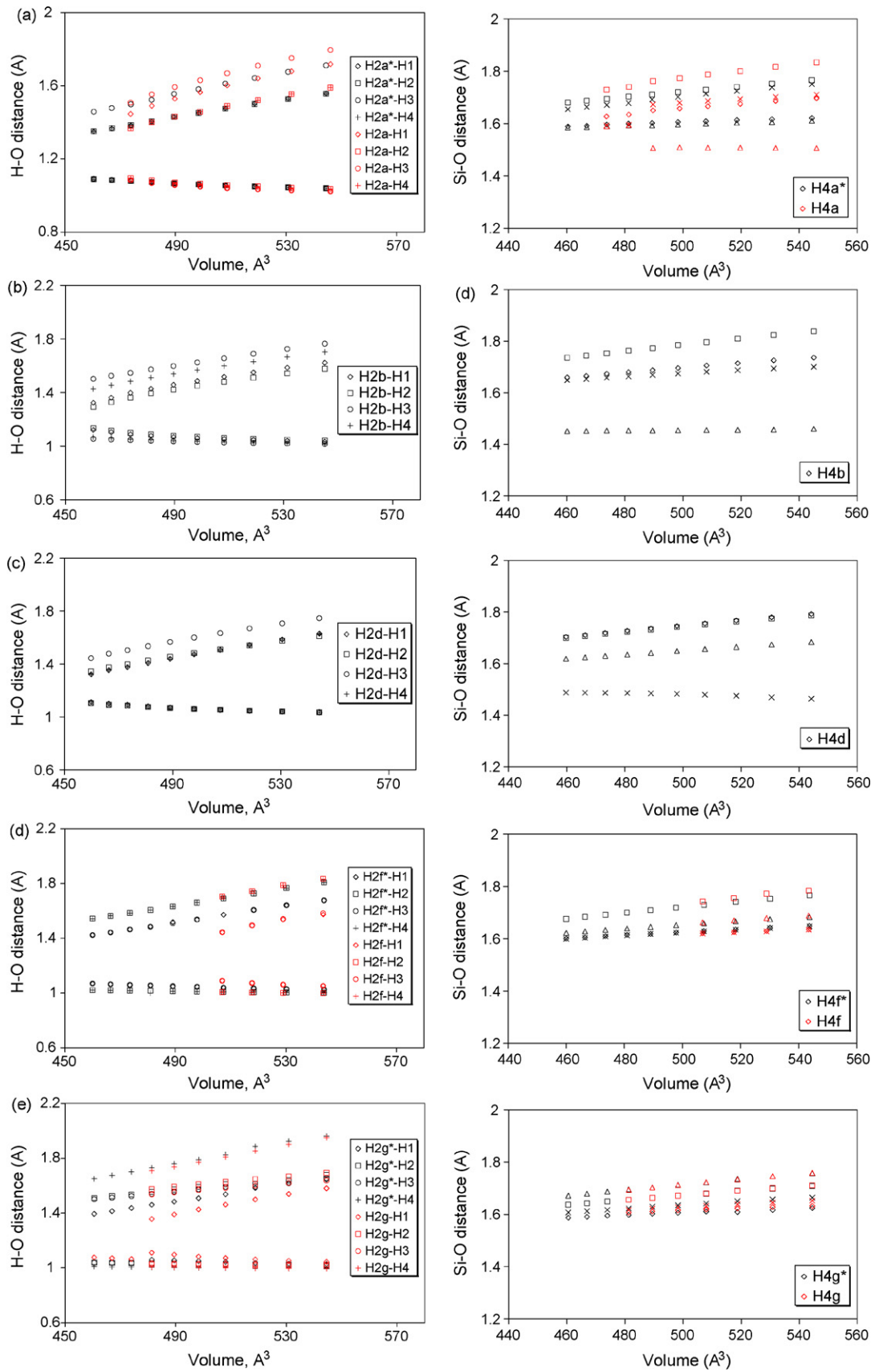


Fig. 9. (a–e) Atom distances for model H4a, H4a*, H4b, H4d, H4f, H4f*, H4g and H4g*. A change of proton sites can be seen from the H–O and Si–O distances of model H4a, H4f and H4g where the red symbols are the less stable configurations. (For interpretation of the references to color in this figure legend, the reader is referred to the web version of the article.)

Table 3
Equation of states for anhydrous and hydrous ringwoodite. The bulk moduli, K_0 and pressure derivative, K'_0 , are from the elastic moduli calculation using a Murnaghan equation of state. References: 1 (Kiefer et al., 1997); 2 (Li et al., 2006); 3 (Weidner et al., 1984); 4 (Li, 2003); 5 (Sinogeikin et al., 2003); 6 (Smyth et al., 2004); 7 (Jacobsen et al., 2004); 8 (Inoue et al., 1998); 9 (Wang et al., 2003, 2006); 10 (Yusa et al., 2000). This study (H2a*–SiH) and ref1 and ref2 are first-principle calculations at 0 K.

Ref.	V_0 (\AA^3)	H ₂ O (wt%)	K_0 (GPa)	K'	Composition
DRY	539.95	0.00	175	4.06	Dry Mg100
H2a	542.22	1.65	166	3.91	Hydrous Mg100
H4a*	544.43	3.30	159	4.21	Hydrous Mg100
H4f*	544.43	3.30	152	4.16	Hydrous Mg100
SiH	559.75	3.30	142	4.34	Hydrous Mg100
Ref1	497.00	0.00	206	–	Mg100
Ref2	524.56	0.00	198	4.07	Mg100
Ref3	525.30	0.00	184	–	Mg100
Ref4	518.81	0.00	185	4.5	Mg100
Ref5	526.20	0.00	188	4.1	Mg91Fe9
Ref6	530.18	0.93	169	–	Hydrous Mg90Fe10
Ref7	530.80	1.00	176	–	Hydrous Mg89Fe11
Ref8	527.24	2.20	155	–	Hydrous Mg100
Ref9	530.10	2.34	166	4.4	Hydrous Mg100
Ref10	529.79	2.80	148	–	Hydrous Mg100

Table 4
Vibrational modes (cm^{-1}) of Mg₂SiO₄ ringwoodite at ambient conditions. Ref: a (Yu and Wentzcovitch, 2006); b (Chopelas, 2000); c (McMillan and Akaogi, 1987); d (Akaogi et al., 1984).

T2g (R)	Eg (R)	T2g (R)	T2g (R)	Ag (R)	T1u (IR)	T1u (IR)	T1u (IR)	T1u (IR)	Reference
309	375	586	817	831	345	423	549	829	a
302	372	600	796	834					b
302 ^c	370 ^c	600 ^c	794 ^c	836 ^c	350 ^d	445 ^d	545 ^d	830 ^d	c, d
306	372	585	811	828	345	418	545	823	This study

of model SiH (shown in Fig. 5) all have their four protons inside the Si-vacant tetrahedron at all investigated pressures up to 40 GPa. Fig. 10 shows the atom distances for the SiH model. It can be clearly seen that the pressure decreases the distance between the protons and the Si-vacancy in model SiH, but H–O distances have little change. The four protons are located between the Si-vacancy and the four oxygen neighbors. In contrast, hydrogen defects were found along the edge of the tetrahedron in forsterite in the previous study (Brodholt and Refson, 1999).

Blanchard et al. (2009) report similar calculations as the H4 model and the SiH model. While our results generally agree with theirs, they found the H align along the tetrahedral edges. We have

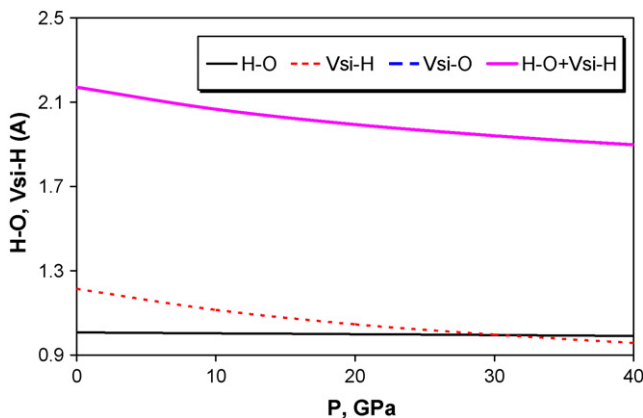


Fig. 10. Bond distances of model SiH vs. pressure. H–O is the average distance between the four protons to the closest oxygen atoms; $V_{\text{Si-H}}$ is the average distance between four protons and the Si-vacancy. $V_{\text{Si-O}}$ is the average distance between Si-vacancies to the four neighbor oxygen atoms. $\text{H-O} + V_{\text{Si-H}}$ is the sum of H–O and $V_{\text{Si-H}}$. The differences among the four H–O and $V_{\text{Si-H}}$ are very small (less than 0.01 Å). These figure indicates that at all pressure investigated, the location of the protons are between the Si-vacancy and its oxygen neighbors.

not been able to reproduce that feature of their model. Lager et al. (1987) report several geometries of the H in the hydrogarnet substitution. Both configurations of H pointing towards the center of the tetrahedron and of H along the edge of the tetrahedron are suggested by the neutron data.

3.6. Vibrational properties

Equations of state for the different configurations are given in Table 3. The bulk moduli, K_0 , and pressure derivatives, K'_0 , are from the elastic moduli calculations. Calculated results are compared with experimental data.

Mg₂SiO₄ ringwoodite belongs to space group $Fd-3m$ (Hazen et al., 1993). At 0 GPa, the IR and Raman modes are caused by the Mg–Si–O framework vibration normal modes and are all less than 1000 cm^{-1} . We list our calculated frequencies of the optical modes of anhydrous ringwoodite at 0 GPa and 0 K in Table 4, and compare with previously reported results at 0 GPa pressure. We find that the vibrational modes of the anhydrous ringwoodite agree remarkably well with the observations.

When we introduce hydrogen defects into the ringwoodite structure, the loss of symmetry makes most of the vibrational modes IR active. However, the notable O–H stretching modes are at wave-numbers greater than 2000 cm^{-1} . Table 5 compares the four unique models (H2a, H4a, H4f and SiH) with the observed data

Table 5
IR O–H stretching modes calculated from the different structural models and the observations of a (Chamorro Pérez et al., 2006). These are the only modes at wavenumbers larger than 2000 cm^{-1} .

O–H stretching mode (cm^{-1})				Model
2435	2445			H2a
2027	2031	2032	2034	H4a
2080	2623	2877	2901	H4f
3895	3895	3897	3900	SiH
2450	2550	3150	3700	Obs, a

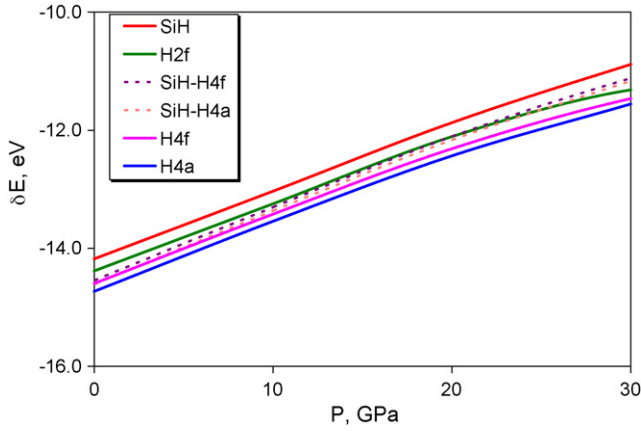


Fig. 11. Energy required to produce one H₂O molecule. The kinetic energy difference between model SiH and model H4a of about 0.6 eV makes SiH less likely to switch with the lowest energy model H4a. However, the model with Mg–Si coupled substitutions such as SiH–H2f, SiH–H4f and SiH–H4a are close to the single-substitution mechanisms (SiH, H2f, H4a and H4f), thus making Si-vacancies likely to coexist with Mg-vacancies.

(Chamorro Pérez et al., 2006). Table 5 illustrates two distinctive features. The first is that despite the similarity of the structure models, the vibrational frequencies are quite different. For example, even though H2a is similar to H4a in that the Mg-vacancies are segregated (do not share an O–O edge); H2a has frequencies around 2400 cm⁻¹; while H4a has frequencies around 2000 cm⁻¹. On the other hand, H4f is the only model that has vibrational frequencies which falls under the observed broad dominant IR absorption band centered around 3150 cm⁻¹; H4f has the two Mg-vacant octahedrons sharing an O–O edge. The highest observed IR absorption band agrees best with SiH stretch modes; SiH has four protons inside the Si-vacant tetrahedral. In conclusion, no single proton incorporation mechanism matches the data: to match the models with the IR observations requires a combination of isolated Mg-vacant octahedra (H2a), coupled Mg-vacancies (H4f) and Si-vacancies (SiH).

Blanchard et al. (2009) find similar results for the predicted IR spectra. They conclude that the SiH vibrations can explain the high frequency IR data. However, they were not able to match the modes around 2500 cm⁻¹, but they did not include the H2a configurations in their consideration.

3.7. Energy comparison of models

The enthalpy (plotted as H–3P for convenience) at 0K of the different models is compared in Fig. 11. The energy difference (δE) is that required to produce one H₂O molecule and are based on the following energy models:

$$\delta E_{(\text{SiH})} = \left(\frac{E(\text{Mg}_{16}\text{Si}_7\text{H}_4\text{O}_{32})_{\text{SiH}} - 8E(\text{Mg}_2\text{SiO}_4)_{\text{ringwoodite}} + E(\text{SiO}_2)_{\text{stishovite}}}{2} \right)$$

$$\delta E_{(\text{H2a})} = (E(\text{Mg}_{15}\text{Si}_8\text{H}_2\text{O}_{32})_{\text{H2a}} - 8E(\text{Mg}_2\text{SiO}_4)_{\text{ringwoodite}} + E(\text{MgO})_{\text{periclase}})$$

$$\delta E_{(\text{SiH-H4f})} = \left(\frac{E(\text{Mg}_{16}\text{Si}_7\text{H}_4\text{O}_{32})_{\text{SiH}} + E(\text{Mg}_{14}\text{Si}_8\text{H}_4\text{O}_{32})_{\text{H4f}} - 15E(\text{Mg}_2\text{SiO}_4)_{\text{ringwoodite}}}{4} \right)$$

$$\delta E_{(\text{SiH-H4a})} = \left(\frac{E(\text{Mg}_{16}\text{Si}_7\text{H}_4\text{O}_{32})_{\text{SiH}} + E(\text{Mg}_{14}\text{Si}_8\text{H}_4\text{O}_{32})_{\text{H4a}} - 15E(\text{Mg}_2\text{SiO}_4)_{\text{ringwoodite}}}{4} \right)$$

$$\delta E_{(\text{H4f})} = \left(\frac{E(\text{Mg}_{14}\text{Si}_8\text{H}_4\text{O}_{32})_{\text{H4f}} - 8E(\text{Mg}_2\text{SiO}_4)_{\text{ringwoodite}} + 2E(\text{MgO})_{\text{periclase}}}{2} \right)$$

$$\delta E_{(\text{H4a})} = \left(\frac{E(\text{Mg}_{14}\text{Si}_8\text{H}_4\text{O}_{32})_{\text{H4a}} - 8E(\text{Mg}_2\text{SiO}_4)_{\text{ringwoodite}} + 2E(\text{MgO})_{\text{periclase}}}{2} \right)$$

Table 6

Elastic properties of hydrous ringwoodite. The cubic elastic moduli (in GPa) for several models of ringwoodite are compared with observations as well as the aggregate elastic properties. Unit cell volume and density are also given. The models are for 0 GPa and 0 K. Observed: a (Weidner et al., 1984); b (Inoue et al., 1998).

	c_{11}	c_{12}	c_{44}	K	G	ρ (g/cm ³)	% H ₂ O
Dry	308	108	112	175	107	3.46	0.00
H2a	292	104	115	166	106	3.38	1.65
H4f	266	96	104	153	96	3.30	3.30
H4a	279	100	109	159	101	3.30	3.30
SiH	255	85	101	142	94	3.27	3.30
Dry a	327	112	126	184	119	3.56	0.00
Wet b	281	92	117	155	108	3.47	2.20

A few points emerge from these energy calculations. First, the energy difference between model SiH and model H4a is equivalent to about 1 eV, which makes SiH substantially less likely than lowest energy model H4a. However, the models with Mg–Si coupled substitutions such as SiH–H4f and SiH–H4a (the classic Schottky defect) are close to the single-substitution mechanisms (H4a and H4f), and thus make it possible for hydrogarnet substitutions to exist with Mg-vacancy substitutions. Samples made at elevated temperature should, therefore, contain a combination of proton incorporation mechanisms. This would be consistent with the observation of Kudoh (2001) who demonstrated that the Si, as well as Mg, was depleted in ringwoodite as H content increased. Furthermore, the silica activity in the system will change the balance between silicon vacancies and magnesium vacancies. Secondly, the energy required to make coupled magnesium vacancies such as H4a and H4f, are lower than required to place the same amount of water in single, non-coupled vacancies, H2a. This suggests that the protons will cluster, forming groups such as H4a or H4f rather dispersing the hydrogen uniformly throughout the structure.

3.8. Elastic properties

The zero pressure 0K single crystal elastic properties of several of the models are given in Table 6 along with the aggregate values. These elastic moduli are based on averaging the 21 elastic moduli of the triclinic unit cell to reflect a random orientation of the hydrogen defects since the introduction of proton defects distorts the unit cell in the calculation. Most of the elastic moduli decrease as the hydrogen content increases. However, c_{44} for model H2a is larger than it is for dry ringwoodite. As illustrated by the three models with 4 H per cell, the elastic properties are sensitive to the structural model. The bulk modulus varies by over 10% among the models and the aggregate shear modulus varies by 6%. In general the impact of the hydrogarnet defects is greater than the magnesium defect for both

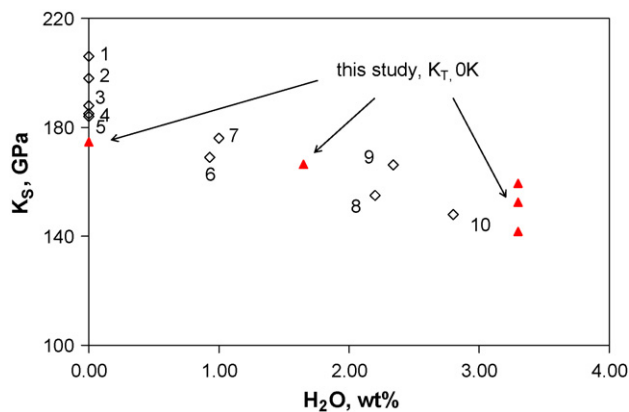


Fig. 12. Bulk modulus as a function of water content. Data for this study are listed in 3. References: 1 (Kiefer et al., 1997); 2 (Li et al., 2006); 3 (Weidner et al., 1984); 4 (Li, 2003); 5 (Sinogeikin et al., 2003); 6 (Smyth et al., 2004); 7 (Jacobsen et al., 2004); 8 (Inoue et al., 1998); 9 (Wang et al., 2003, 2006); 10 (Yusa et al., 2000). Ref1 and Ref2 are first-principle calculations at 0K; Ref10 is KT from volume compression measurement; Ref3–6 are for bulk modulus K_s . The three calculated model bulk moduli at 3.3%, from highest to lowest, are H4a, H4f, SiH.

the volume and the elastic property. The variation of bulk modulus with water content is illustrated in Fig. 12. Theory and observations agree quite well. The bulk modulus for the theory depends on the particular structural model, but is generally consistent with a decrease of bulk modulus by 7.1 GPa for each percent of water in the structure.

The effect of the hydrogen defect on elastic wave velocities is mitigated by the compensation of elastic modulus decrease by density decrease. Fig. 13 illustrates the pressure dependence of aggregate sound wave velocities. For longitudinal velocities, the dry sample is very similar to H2a and H4a, while both H4f and the hydrogarnet model (SiH) have a significantly reduced velocity. In

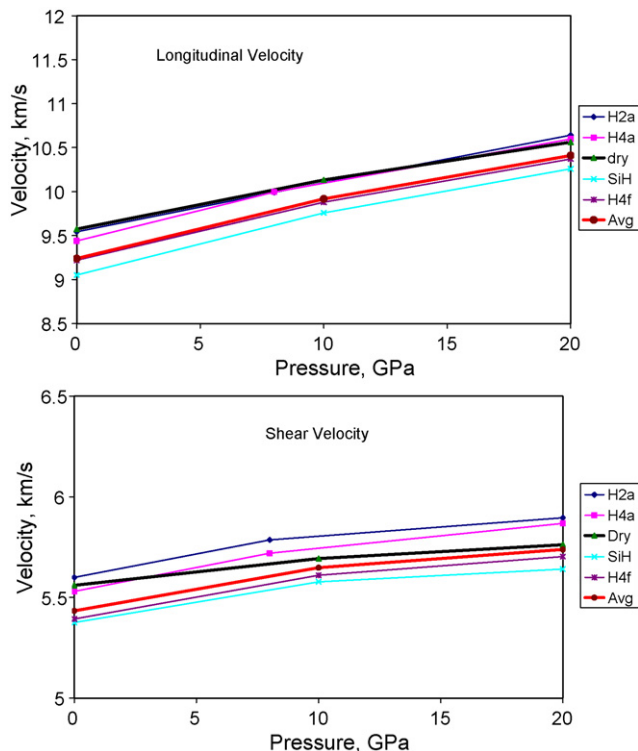


Fig. 13. Acoustic velocities as a function of pressure for the various structural models. The Avg model is an average of H4a, H4f, and SiH.

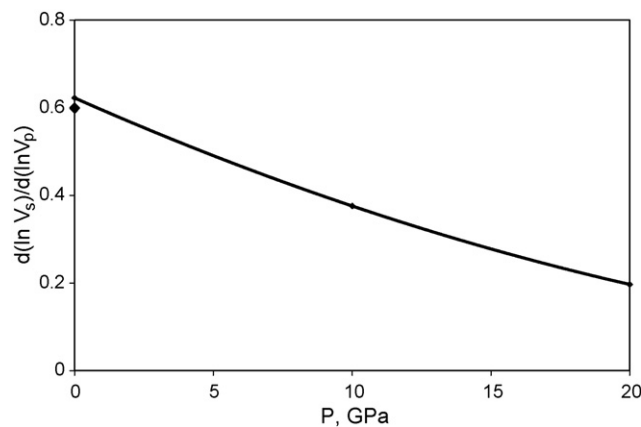


Fig. 14. $d \ln V_s / d \ln V_p$ as a function of pressure. These are calculated by comparing the average four hydrogen models with the dry model. The black diamond is experimental data obtained by combining the ringwoodite data of Inoue et al. (1998) and Weidner et al. (1984).

the case of the shear wave, the effect of water varies depending on the particular mechanism. Dry ringwoodite is actually slower than H2a and H4a for most of the pressure range, while H4f and SiH are slower than dry ringwoodite, as is normally expected. Thus a mixed population of these hydrogen defects should lower the acoustic velocities, but the amount of decrease will depend on the distribution among the defect sites. Also illustrated in Fig. 13 is the velocity for the average of the three models with 4 H substitution (Avg) generated by averaging the elastic moduli. This is deemed a reasonable model as their enthalpies are very similar. The shear velocities of the dry and Avg models converge by about 25 GPa. Fig. 14 illustrates the pressure dependence of the quantity $d \ln V_s / d \ln V_p$ due to water variations. Also plotted is the room pressure experimental data using the results of Weidner et al. (1984) for the dry ringwoodite and Inoue et al. (1998) for hydrated ringwoodite. As seen here, this quantity is less than 1 and decreases with pressure. This low value is unusual for this quantity as most driving parameters such as temperature or iron content yield a value greater than one. We suggest that this parameter can be used to define regions in the Earth where the water content is driving lateral variations in seismic velocity.

3.9. *Ab initio* molecular dynamics simulation

To characterize the dynamics of protons in ringwoodite, AIMD simulations were performed. These were run for over 3 ps after equilibrating the system at temperatures of 1000 and 2000 K. We used model H2a. Similar to the reported dynamic behavior of protons in wadsleyite (Haiber et al., 1997), the dynamics of the protons at high temperature give rise to highly inharmonic motion both in bending and stretching, as shown in Fig. 15. No diffusion of protons was observed at temperature up to 2000 K. The two equivalent energy minimum sites for proton have dOH of ~ 1.1 and 1.5 Å. The protons cross between the double wells of the potential (the two sites between O–O pairs) more frequently with increasing pressure and temperature. The bending angle of proton changes with pressure and temperature but average around $\sim 160^\circ$. The proton stays in the Mg–vacant octahedron during the sampling time but not attach to a unique O–O pair. However, the two protons do not share an oxygen host. Calculations for the SiH model demonstrates that, when associated with a silicon vacancy, the protons stay within the tetrahedral with the O–H bond oriented towards the vacant Si position.

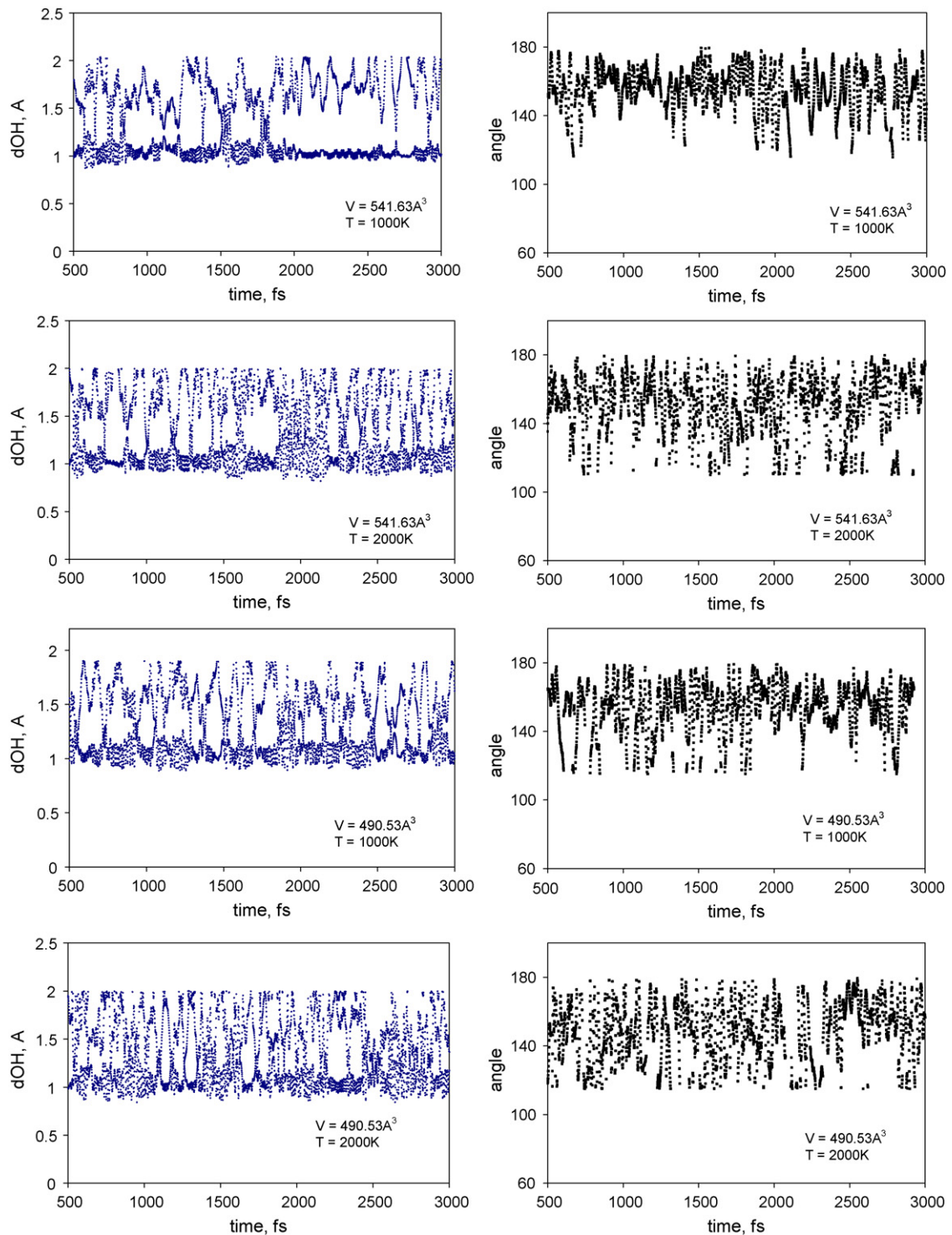


Fig. 15. Dynamics of a proton between two oxygen atoms in ringwoodite (model H2a) at two temperatures and volumes. There are two equivalent minima $d(\text{OH})$ of ~ 1.1 and ~ 1.5 Å. The bending motion of a proton is shown as the O–H–O angle.

4. Summary

The protonation sites of hydrous ringwoodite have been studied using *ab initio* methods. In the case when they replace a magnesium cation, the protons tend to be stable at one of the minima between O–O edge and stay within the Mg-vacant octahedron. There are many possible meta-stable protonation sites. The higher the temperature, the more frequently protons switch between the possible six O sites, but they always remains in the Mg-vacant octahedron.

Both temperature and pressure have an effect on the stretching and the bending motion of the protons in Mg_2SiO_4 ringwoodite. The total energies of some proton sites, especially between the two energy minima between the O–O pair, are low enough to be exchangeable at Earth conditions. The O–H distance (~ 1.1 Å) is not as sensitive to pressure as the O...H distance is. In the case where the protons substitute for silicon, four protons reside within the vacant tetrahedron, with the O–H bond pointing towards the center of the tetrahedron.

Energy considerations suggest that hydrogen clusters with substitutions of Mg by two protons being the most stable state. If the octahedra share one edge, then the energy is slightly higher. Isolated octahedra have even higher energy for the same amount of H. The highest energy state is that of the Si replacement by four protons. However, a coupled replacement of one Si and two Mg by eight protons has only a slightly higher energy than the lowest energy substitution. The ordering of energies of the total system will be influenced by the Si fugacity in the system. Excess MgO will favor the formation of Si-vacancies while excess Si will favor the Mg-vacancy.

The predicted IR stretching modes are quite different for the different structural models. Comparison with observations suggests that a combination of H2a, H4f, and SiH models is present in that specific sample of hydrous ringwoodite.

The bulk modulus is sensitive to the proton concentration, defined as $K = -7.1C_{\text{H}_2\text{O}}(\text{wt}\%) + 175 \text{ GPa}$ by this study. The calculated water concentration derivative of bulk modulus ($-7.1 \text{ GPa/wt}\%$) is consistent with the reported experimental data. The shear modulus depends more strongly on the particular structural model with some mechanism actually resulting in larger shear moduli.

The unusually low value of $(d \ln V_S/d \ln V_P)$ induced by water variation suggests a potentially important diagnostic for the variation of water in the transition zone. The room pressure data agree with the calculations, and the calculations suggest that this value decreases with pressure. We expect that temperature will have an affect similar to the inverse of pressure, with volume being the main controlling variable.

Density also decreases with increasing water content. Combined with the elastic properties, the effect of water on sound velocity depends on the substitution model. H2a and H4a yield a greater shear velocity over a wide pressure range than do dry ringwoodite and nearly the same longitudinal velocity. In contrast, both H4f and SiH yield lower velocities. These results suggest that the effect of water in ringwoodite on seismic velocities will depend on the Si fugacity of the system and the water content of the ringwoodite.

Acknowledgements

This work is support by NERC (Grant Nos. NER/T/S/2001/00855; NER/O/S/2001/01227), and computer facilities provided by NERC at University College London, and the UK National Supercomputing Service (Hector). We acknowledge NSF EAR-9909266, EAR0135551, EAR00135550, EAR1073469, and EAR0809397.

References

Akaogi, M.N., Ross, L., McMillan, P., Navrotsky, A., 1984. The Mg_2SiO_4 polymorphs (olivine, modified spinel and spinel)—thermodynamic properties from oxide melt solution calorimetry, phase relations, and models of lattice vibrations. *American Mineralogist* 69, 499–512.

Alfè, D., 1999. Ab-initio molecular dynamics, a simple algorithm for charge extrapolation. *Computer Physics Communications* 118, 31–33.

Baroni, S., Dal Corso, A., de Gironcoli, S., Giannozzi, P., 2001. Phonons and related crystal properties from density-functional perturbation theory. *Reviews of Modern Physics* 73 (2), 515 LP–562 LP.

Bercovici, D., Karato, S.-i., 2003. Whole-mantle convection and the transition-zone water filter. *Nature* 425, 39–44.

Blanchard, M., Balan, E., Wright, K., 2009. Incorporation of water in iron-free ringwoodite: a first-principles study. *American Mineralogist* 94, 83–89.

Blöchl, P.E., 1994. Projector augmented-wave method. *Physical Review B* 50, 17953–17979.

Bolfan-Casanova, N., Keppler, H., Rubie, D.C., 2000. Water partitioning between nominally anhydrous minerals in the $\text{MgO-SiO}_2\text{-H}_2\text{O}$ system up to 24 GPa: implications for the distribution of water in the Earth's mantle. *Earth and Planetary Science Letter* 182, 209–221.

Brodholt, J.P., Refson, K., 1999. An ab initio study of hydrogen in forsterite and a possible mechanism for hydrolytic weakening. *Journal of Geophysical Research* 105 (B8), 18977–18982.

Carrez, P., Cordier, P., Mainprice, D., Tommasi, A., 2006. Slip systems and plastic shear anisotropy in Mg_2SiO_4 ringwoodite: insights from numerical modelling. *European Journal of Mineralogy* 18, 149–160.

Ceperley, D.M., Alder, B.J., 1990. Ground state of the electron gas by a stochastic method. *Physical Review Letter* 45, 566–569.

Chamorro Pérez, E.M., et al., 2006. Synchrotron IR study of hydrous ringwoodite ($\gamma\text{-Mg}_2\text{SiO}_4$) up to 30 GPa. *Physics and Chemistry of Minerals* 33, 502–510.

Chen, J., Weidner, D.J., Vaughan, M., 1998. Strength and water weakening of mantle minerals, olivine, wadsleyite and ringwoodite. *Geophysical Research Letters* 25 (4), 575–578.

Chopelas, A., 2000. Thermal expansivity of mantle relevant magnesium silicates from vibrational spectroscopy at high pressures. *American Mineralogist* 85, 270–278.

Haiber, M., Ballone, P., Parrinello, M., 1997. Structure and dynamics of protonated Mg_2SiO_4 : an ab-initio molecular dynamics study. *American Mineralogist* 82, 913–922.

Hazen, R.M., Downs, R.T., Finger, L.W., Ko, J., 1993. Crystal chemistry of ferromagnesian silicate spinels: evidence for Mg-Si disorder. *American Mineralogist* 78, 1320–1323.

Huang, X., Xu, Y., Karato, S.-i., 2005. Water content in the transition zone from electrical conductivity of wadsleyite and ringwoodite. *Nature* 434, 746–749.

Inoue, T., Weidner, D.J., Northrup, P.A., Parise, J.B., 1998. Elastic properties of hydrous ringwoodite (gamma-phase) in Mg_2SiO_4 . *Earth and Planetary Science Letters* 160 (1–2), 107–113.

Jacobsen, S.D., Smyth, J.R., Spetzler, H., Holl, C.M., Frost, D.J., 2004. Sound velocities and elastic constants of iron-bearing hydrous ringwoodite. *Physics of the Earth and Planetary Interiors* 143–44, 47–56.

Karki, B.B., Wentzcovitch, R.M., Gironcoli, S., Baroni, d.S., 2000. Ab initio lattice dynamics of MgSiO_3 perovskite at high pressure. *Physical Review B* 62 (22), 14750.

Kavner, A., 2003. Elasticity and strength of hydrous ringwoodite at high pressure. *Earth and Planetary Science Letters* 214 (3–4), 645–654.

Kiefer, B., Stixrude, L., Wentzcovitch, R.M., 1997. Calculated elastic constants and anisotropy of Mg_2SiO_4 spinel at high pressure. *Geophysical Research Letters* 24 (22), 2841–2844.

Kleppe, A.K., Jephcoat, A.P., Smyth, J.R., 2002a. Raman spectroscopy study of hydrous gamma- Mg_2SiO_4 to 56.5 GPa. *Physics and Chemistry of Minerals* 29, 473–476.

Kleppe, A.K., Jephcoat, A.P., Smyth, J.R., Frost, D.J., 2002b. On protons, iron and the high-pressure behavior of ringwoodite. *Geophysical Research Letters* 29 (21), 2021, doi:10.1029/2002GL015276.

Kohlstedt, D.L., Keppler, H., Rubie, D.C., 1996. Solubility of water in the alpha, beta and gamma phases of $(\text{Mg,Fe})_2\text{SiO}_4$. *Contributions to Mineralogy and Petrology* 123 (4), 345–357.

Kresse, G., Joubert, D., 1999. From ultrasoft pseudopotentials to the projector augmented-wave method. *Physical Review B* 59, 1758–1775.

Kudoh, V., 2001. Structural relation of hydrous ringwoodite to hydrous wadsleyite, $\text{Mg}_{1.75}\text{SiH}_{0.5}\text{O}_4$: possible hydrous magnesium silicate in the mantle transition zone. *Physics and Chemistry of Minerals* 28 (8), 523–530.

Kudoh, Y., Inoue, T., Arashi, H., 1996. Structure and crystal chemistry of hydrous wadsleyite. *Physics and Chemistry of Minerals* 23 (7), 461–469.

Kudoh, Y., Kuribayashi, T., Mizobata, H., Ohtani, E., 2000. Structure and cation disorder of hydrous ringwoodite, gamma- $\text{Mg}_{1.89}\text{Si}_{0.98}\text{H}_{0.30}\text{O}_4$. *Physics and Chemistry of Minerals* 27 (7), 474–479.

Lager, G.A., Armbruster, T., Faber, J., 1987. Neutron and X-ray diffraction study of hydrogarnet $\text{Ca}_3\text{Al}_2(\text{O}_4\text{H}_4)_3$. *American Mineralogist* 72, 756–765.

Li, B., 2003. Compressional and shear wave velocities of ringwoodite gamma- Mg_2SiO_4 to 12 GPa. *American Mineralogist* 88, 1312–1317.

Li, L., Weidner, D.J., Brodholt, J., Alfè, D., Price, G.D., 2006. Elasticity of Mg_2SiO_4 ringwoodite at mantle conditions. *Physics of the Earth and Planetary Interior* 157 (3–4), 181–187.

Li, L., Carrez, P., Weidner, D.J., 2007. Effect of cation ordering and pressure on spinel elasticity by ab initio simulation. *American Mineralogist* 92, 174–178.

Manghnani, M.H., et al., 2005. Equation of state of hydrous FO_{90} ringwoodite to 45 GPa by synchrotron powder diffraction. *Mineralogical Magazine* 69 (3), 317–323.

McMillan, P., Akaogi, M., 1987. Raman spectra of beta- Mg_2SiO_4 (modified spinel) and gamma- Mg_2SiO_4 (spinel). *American Mineralogist* 72, 361–364.

Perdew, J.P., Zunger, A., 1981. Self-interaction correction to density-functional approximations for many-electron systems. *Physical Review B* 23, 5048.

Ross, N.L., Gibbs, G.V., Rosso, K.M., 2003. Potential docking sites and positions of hydrogen in high-pressure silicates. *American Mineralogist* 88, 1452–1459.

Sinogeikin, S.V., Bass, J.D., Katsura, T., 2003. Single-crystal elasticity of ringwoodite to high pressures and high temperatures; implications for 520 km seismic discontinuity. *Physics of the Earth and Planetary Interiors* 136 (1–2), 41–66.

Smyth, J.R., 1994. A crystallographic model for hydrous wadsleyite (beta- Mg_2SiO_4)—an ocean in the Earth's interior. *American Mineralogist* 79 (9–10), 1021–1024.

Smyth, J.R., Holl, C.M., Frost, D.J., Jacobsen, S.D., 2004. High pressure crystal chemistry of hydrous ringwoodite and water in the Earth's interior. *Physics of the Earth and Planetary Interiors* 143–44, 271–278.

Troullier, N., Martins, J.L., 1991. Efficient pseudopotential for plane wave calculations. *Physical Review B* 43, 1993–2006.

Tsuchiya, J., Tsuchiya, T., Wentzcovitch, R.M., 2005. Vibrational and thermodynamic properties of MgSiO_3 post-perovskite. *Journal of Geophysical Research* 110, B02204/1–6.

- Wang, J.Y., Sinogeikin, S.V., Inoue, T., Bass, J.D., 2003. Elastic properties of hydrous ringwoodite. *American Mineralogist* 88 (10), 1608–1611.
- Wang, J.Y., Sinogeikin, S.V., Inoue, T., Bass, J.D., 2006. Elastic properties of hydrous ringwoodite at high-pressure conditions. *Geophysical Research Letters* 33 (14).
- Weidner, D.J., Sawamoto, H., Sasaki, S., 1984. Single-crystal elastic properties of the spinel phase of Mg_2SiO_4 . *Journal of Geophysical Research* 89 (B9), 7852–7860.
- Wentzcovitch, R.M., Price, G.D., 1996. High pressure studies of mantle minerals by ab initio variable cell shape molecular dynamics. In: Silvi, B., Darco, P. (Eds.), *Molecular Engineering*. Kluwer Academic Publication, Dordrecht.
- Wentzcovitch, R.M., Ross, N.L., Price, G.D., 1995. Ab initio study of MgSiO_3 and CaSiO_3 perovskites at lower-mantle pressures. *Physics of the Earth and Planetary Interiors* 90 (1–2), 101–112.
- Yu, Y.G., Wentzcovitch, R.M., 2006. Density functional study of vibrational and thermodynamic properties of ringwoodite. *Journal of Geophysical Research-Solid Earth and Planets* 111, B12202, doi:10.1029/2006JB004282.
- Yusa, H., Inoue, T., Ohishi, Y., 2000. Isothermal compressibility of hydrous ringwoodite and its relation to the mantle discontinuities. *Geophysical Research Letters* 27 (3), 413–416.